Setup and characterisation of a gas mixing unit for the dilution of CO_2 with N_2

Bachelor thesis by

Luana Rubino

November 5, 2020

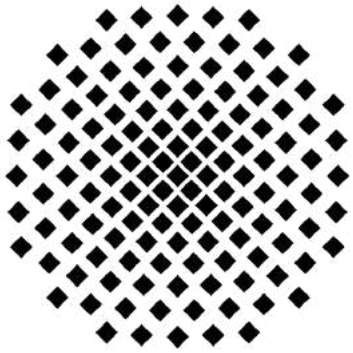

University of Stuttgart

Faculty 08

5th Institute of Physics

Examinar Prof. Dr. Tilman Pfau

Erklärung

Hiermit erkläre ich, dass nach der Prüfungsordnung der Universität Stuttgart für den Bachelorstudiengang Physik vom 31. Juli 2015 nach §27 Absatz 7 die Bachelorarbeit die folgende Punkte versichert

- dass die Arbeit selbständig verfasst wurde,
- dass keine anderen als die angegebenen Quellen benutzt und alle wörtlich oder sinngemäß aus anderen Werken übernommenen Aussagen als solche gekennzeichnet sind,
- dass die eingereichte Arbeit weder vollständig noch in wesentlichen Teilen Gegenstand eines anderen Prüfungsverfahren gewesen ist, und
- dass das elektronische Expemplar mit den anderen Exemplaren übereinstimmt

Luana Rubino
Stuttgart den 05. November 2020

Deutsche Zusammenfassung

Ziel dieser Arbeit war es, ein Gasmischsystem für die Gase NO und N_2 aufzubauen und zu planen. Da die Struktur mit Rohren zusammengebaut ist, sollte hierfür der Durchmesser bestimmt werden, was in Kapitel 2 mit der Berechnung der Knudsen-Zahl Kn und der Reynolds-Zahl Re erfolgt.

Für eine laminare Strömung kann in diesem Aufbau ein Durchmesser von $d = 4\,\text{mm}$ zugewiesen werden. Für einen konstanten Durchfluss werden Massendurchflussregler (MFCs) verwendet, um unterschiedliche Mischungsverhältnisse zu erzeugen. Die Funktionsweise wird in Abschnitt 3.1 betrachtet. Sie basiert auf der thermischen Massenbewegung, die mit Hilfe der spezifische Wärmekapazität in einen Massedurchfluss umgerechnet werden kann. Zur Messung der Konzentration nach den MFCs wird ein CO_2 Sensor verwendet, der die Infrarotabsorption der Moleküle misst was im Kapitel 3.4 näher erläutert wird. Für die Untersuchung des Systems, das für N_2 und NO Gas ausgelegt ist, werden Messungen mit CO_2 und N_2 Gas durchgeführt, da es einfacher zu handhaben ist als NO Gas.

In Kapitel 4 *Messungen und Auswertungen* werden die MFCs und der CO_2 Sensor untersucht. Bei der Untersuchung des CO_2 Sensors während der Aufzeichnung der Daten wurde festgestellt, dass die lange Zeitverzögerung auf die Tatsache zurückzuführen ist, dass es einige Zeit dauert, bis eine festgelegte Gleichgewichtskonzentration im CO_2 Sensor vorliegt, die nicht optimal ist, da die Mischverhältnisse nicht nach einer beliebigen Zeit verändert werden konnten. Die MFCs wurden bei der Untersuchung der Kombinationen auf konstante Konzentrationen berücksichtigt, was dazu geführt hat, dass für 2000 ppm und 4000 ppm CO_2 in Bezug auf den Gesamtfluss F_{tot} beobachtet wurde. In allen gemessenen Daten hat der CO2-Sensor einen sehr hohen Einfluss auf die Fehlerbalken, die fast ausschließlich aus dem Sensorfehler bestehen, was die Auswertung der MFCs nicht vereinfacht.

Das mit Mathematica gelöste Skript in Anhang 2 bietet eine analytische Lösung für die MFCs. Hier werden die Kombinationen von MFCs ohne Sensor betrachtet, hierzu werden die Bilder in Abschnitt 4.3 gezeigt. Die Abbildungen zeigen deutlich den kleinsten Fehler für die jeweiligen Kombinationen zweier MFCs für einen Gesamtfluss von $F_{\text{tot}} = 1000\,\text{sccm}$ und eine Verdünnung von $D_2 = 1/1000$.

Contents

1 Introduction

Nitric oxide (NO) is a linear molecule found in many biological and chemical processes [1]. Apart from various processes in the human body, NO can be synthesized from the aminoacid L-arginine [2]. It is known that the concentration of NO of the exhaled air gives information about the inflammatory status of the airway for asthma patients [3]. For detailed information about the amount of the NO concentration in the exhaled breath, breath gas analysis is necessary. This gas analysis can be done with an NO sensor, for example with a optogalvanic sensor [1], which optically excites NO to a Rydberg state [30] by collisions with ions and the background gas, which then measures the resulting charges. The approximated detection limit of this sensor is at 5 ppb [1].

The gas mixing system built here is one part of a large project that deals with trace gas. The gas mixing system is there to generate known mixing ratios between NO and N_2 which the NO sensor can then measure. The sensitivity of the NO sensor can be improved by reducing the sample volume.

It is known that NO is toxic in high amounts which makes experimenting with it dangerous. This is the reason why this thesis uses CO_2 instead of NO for testing the gas mixing unit with a known sample. Another advantage of this is that CO_2 sensors are cheaper than NO sensors. Since the only thing that differs in the setup is the type of sensor needed, the setup for the characterization of the gas mixing unit stays the same. Because an optogalvanic gas sensor measures the concentration of the trace gas (NO or CO_2), a constant mass flow is essential for achieving reliable results. This thesis is an attempt to achieve a specific mixing ratio with constant mass flow by utilizing four different mass flow controllers (MFC).

This thesis begins with a theoretical background where an overview of different gas models is given. In this section, it is discussed why the mixed gases used in this thesis can be approximated as ideal gases. The basic principle of a non-dispersive infrared (NDIR) gas sensor and a MFC is discussed there, too.

After that the setup is described component by component. It begins with the MFCs, their internal setup and technical information. The measurement technique is explained in detail. A description of the gas pipe system built for this thesis follows. It is made clear which components are needed to get laminar flow. Based on that the requirements to the valves are given since they have to be NO resistant. In the last section the principle of the used CO_2 sensor is explained followed by its physical background.

In the measurements and evaluation chapter an interpretation of the measured data is given. This contains a brief characterisation of the CO_2 sensor, the flow changing behavior of different MFCs combinations and the dependency on the concentration change for the forward and backwards direction of the CO_2 sensor.

2 Theoretical Background

This chapter gives an overview about the movements of gases, as well as the laws of gases. Also important is the technology how a non-dispersive infrared gas sensor measures and finally the heat capacity is considered.

The following explanation is mostly based on [4].

2.1 Movements of gases

A closer look into gas dynamics shows that there are two significant flow types: molecular and viscose flow. These types are observed in a pipe with a volume V, the cross-section A and length h.

The molecular flow dominates at low pressure where the mean free path is much larger compared to the pipe diameter. The only interaction the molecules have is with the pipe. In case of the viscose flow type, the pressure is much higher. This means the mean free path is much smaller and the probability of molecules hitting each other is much higher.

To distinguish the molecular flow and the viscose flow the Knudsen number Kn is introduced. The Knudsen flow describes the interaction with the pipe and molecules more or less equally weighted. Therefore, the Knudsen number can be calculated to determine whether the flow is molecular or viscose.

The Knudsen number Kn is defined as:

$$Kn \equiv \frac{\lambda}{l} \tag{2.1}$$

In equation (2.1) λ is the mean free path of the molecules in meters and l is a representative physical length scale in meters. For example for a pipe, l it is the diameter. A number between $Kn = 0.5$ to $Kn = 0.01$ defines a Knudsen flow. If $Kn > 0.5$ it describes molecular flow, for $Kn < 0.01$ it is viscose flow.

As an overview, table 2.1 gives Knudsen numbers for different pipe diameters. The mean free path for CO_2 is $\lambda_{CO_2} = 45\,\text{nm}$ [17] at temperature $T = 20\,°\text{C}$ and a pressure of $p_1 = 1\,\text{bar}$. For $p_2 = 10\,\text{mbar}$ and $T = 20\,°\text{C}$ the mean free path is $\lambda_{CO_2} = 4.5\,\mu\text{m}$ [17].

Table 2.1: Knudsen numbers of CO_2 for different pipe diameters

l [mm]	2	3	4	5	6	7	8	9	10
Kn_1 $[10^{-5}]$	2.25	1.5	1.125	0.9	0.75	0.64	0.5625	0.50	0.45
Kn_2 $[10^{-5}]$	225	150	112.5	90	75	64.3	56.25	50	45

Another important property is the characterisation of gases with a viscose flow, where the speed through the pipe is important. Considering the speed, there are two significant gas flow models: the laminar flow and the turbulent flow. In figure 2.1c) turbulent flow is visualised. As the name indicates it is a turbulent flow what means that here vortices arise. This happens when the center of the pipe and the edges have a huge difference in velocity. In case of big velocity differences it happens that the middle and the edges of the pipe generate friction forces which lead to turbulent flow. For laminar flow the velocity difference is much less which leads to no turbulent flow. Laminar flow is often described as layers with different velocities like the arrows in figure 2.1b). Here the velocity slows down on the edges but is parallel to the other layers.

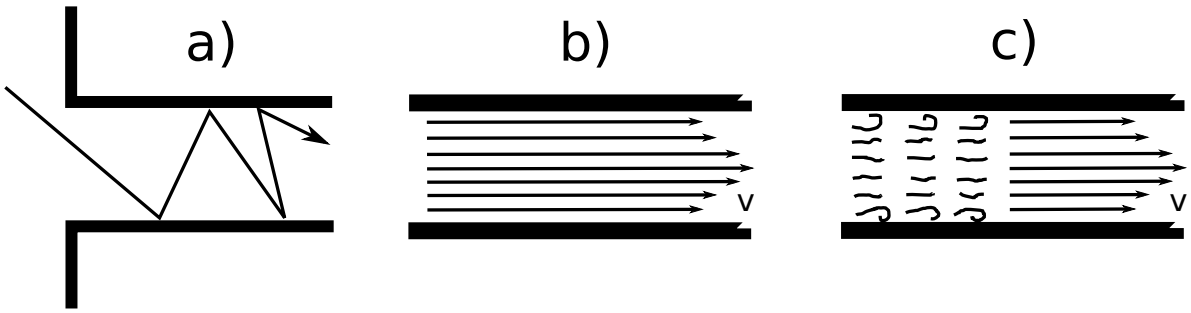

Figure 2.1: This figure describes three different flow types. a) the gas flow enters the pipe and collides with the inner wall of the pipe which is called molecular or ballistic flow. b) shows a laminar flow whereby the velocity vectors are pointing in the same direction, no vertices arise because friction forces to each other are very low. c) shows turbulent behavior which happens due to high velocity of the gas which means the velocity difference between the middle of the pipe and the edges is high. At this picture the length of the vector is proportional to the speed. The type of flow does not only depend on the speed, which can be read from the Reynolds number, the diameter, the dynamic viscosity and the density are also relevant. After [4].

The Reynolds number Re indicates whether the flow is laminar or turbulent. The Reynolds number is defined as

$$Re \equiv \frac{\rho}{\mu} \cdot v \cdot l. \tag{2.2}$$

In equation (2.2) ρ is the density in $[\mathrm{kgm}^{-3}]$, μ the dynamic viscosity in $[\mathrm{kg\,m^{-1}\,s^{-1}}]$, v the flow velocity in $[\mathrm{m\,s^{-1}}]$ and l a representative physical length scale in [m]. A Reynolds

number higher than 4000 defines a turbulent flow and a Reynolds number smaller 2300 defines a laminar flow. Inside of this range it is called Reynolds flow.

The velocity v can be calculated by the time derivative of the Volume V divided by the cross-section area A of the pipe. Now the Reynolds number can be described like in equation (2.3) where h is the length of the pipe. It depends on the diameter l and the time t the gas particles take to pass through the pipe.

$$v = \frac{\dot{V}}{A} = \frac{h}{t} \qquad \Rightarrow \quad Re = \frac{\rho h l}{\mu t} \tag{2.3}$$

As an example CO_2 has the density $\rho = 1.815\,\mathrm{kg/m^3}$ and the dynamic viscosity $\mu = 14.69 \cdot 10^{-6}\mathrm{kg\,m^{-1}\,s^{-1}}$ at pressure $p = 1\,\mathrm{bar}$ and temperature $T = 20\ °\mathrm{C}$ [18]. A few Reynolds numbers of CO_2 are shown in table 2.2.

Table 2.2: Reynolds numbers of CO_2 for different pipe diameters l and different flow times t at the length of $h = 4\,\mathrm{m}$.

$v\ [\mathrm{m\,s^{-1}}]$	Re_{CO_2}	$l = 3\,\mathrm{mm}$	$4\,\mathrm{mm}$	$5\,\mathrm{mm}$
1.33	$t = 3\,\mathrm{s}$	4942	6589	8236
1	$4\,\mathrm{s}$	3706	4942	6177
0.8	$5\,\mathrm{s}$	2965	3953	4942
0.66	$6\,\mathrm{s}$	2471	3294	4118
0.57	$7\,\mathrm{s}$	2118	2824	3530
0.5	$8\,\mathrm{s}$	1853	2471	3088
0.44	$9\,\mathrm{s}$	1647	2196	2745

2.2 Ideal gas

An ideal gas describes an idealized representation of the gas, whereby the gas molecules are viewed as point particles which move statistically. After and before the collision, they move evenly and independently. These point particles can elastically collide with each other and thus transfer energy. Because these are seen as point particles, the only energy they exchange is the kinetic energy. Forces acting on one another, such as the Van-der-Walls force, are not taken into account here. The basic equation for gases which is valid for moving points as particles is known as the ideal gas law (2.4).

$$pV = Nk_\mathrm{B}T \tag{2.4}$$

In equation (2.4), p describes the pressure in [bar], V the volume in [$\mathrm{m^3}$], N the number of molecules, $k_\mathrm{B} = 1.3806 \cdot 10^{-23}\ \mathrm{m^2kg/s^2K}$ the Boltzmann constant and T the temperature in [K]. The ideal gas law is a combination of Boyle-Mariotte's law, Gay-Lussac's law, and Avogadro's law. Boyle-Mariotte's law means that at a given temperature T the volume

is reversely proportional to the pressure p as defined in equation (2.5). Gay-Lussac's law describes a proportionality between the volume and the temperature T as defined in equation (2.6) while the pressure is constant. The last essential law is described by Avogadro, saying that the volume V is proportional to the number of particles n for constant pressure p as well as for constant temperature T (2.7).

$$V \propto \frac{1}{p} \quad : \text{Boyler-Mariotte's law} \tag{2.5}$$

$$V \propto T \quad : \text{Gay-Lussac's law} \tag{2.6}$$

$$V \propto n \quad : \text{Avogadro's law} \tag{2.7}$$

2.3 Real gas

The following explanation is mostly based on [13].

The ideal gas law is valid for moving points which do only interact fully elastic. Real gases instead have extended particles where different forces between the molecules can arise. Attraction and repulsive forces are present, in the following the attraction Van-der-Waals force is considered.

A closer look into the Van-der-Waals force, which describes a very weak force where the interaction between dipoles is considered. The Van-der-Waals force gives a volume and pressure adjustment of the ideal gas law. For molecules, the real volume is $(V - nb)$ with b as the molecules own volume, while the real pressure becomes $\left(p + a\left(\frac{n}{V}\right)^2\right)$ with a as the aspect ratio factor. Equation (2.8) shows the real gas law, with n as amount of substance and a, b as Van-der-Waals constants.

$$\left(p + a\left(\frac{n}{V}\right)^2\right) \cdot (V - nb) = Nk_{\mathbf{B}}T \tag{2.8}$$

2.4 Thermal particles

The following explanation is mostly based on [6] and [7].

Particle velocity

In reality, there are inelastic collisions between particles which lead to a velocity distribution described by the Maxwell-Boltzmann-distribution $f(v)$ as defined in equation

(2.9) with m as mass in [kg] of the particle.

$$f(v) = 4\pi v^2 \left(\frac{m}{2\pi k_\mathrm{B} T}\right)^{\frac{3}{2}} e^{\frac{-mv^2}{2k_\mathrm{B}T}} \tag{2.9}$$

As for every probability distribution there is a most probable value of the velocity as defined in equation (2.10) and an average velocity as defined in equation (2.11). These values are proportional to $\sqrt{T}$, for larger temperatures the probability distribution $f(v)$ gets wider whereby the average speed shifts to a higher speed what figure 2.2 shows.

$$\hat{v} = \sqrt{\frac{2k_\mathrm{B}T}{m}} \tag{2.10}$$

$$\overline{v} = \int_0^\infty v f(v) \mathrm{d}v = \sqrt{\frac{8k_\mathrm{B}T}{\pi m}} \tag{2.11}$$

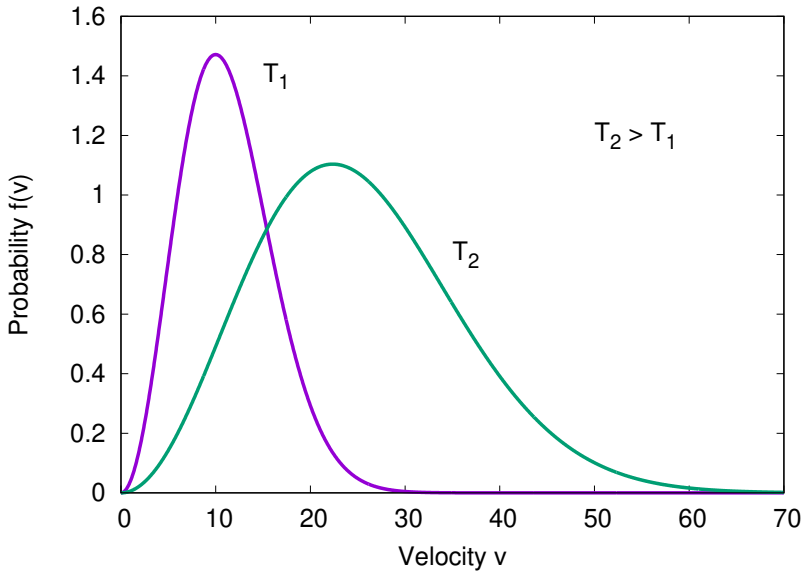

Figure 2.2: The probability $f(v)$ is plotted against the velocity v for two different temperatures T_1 and T_2. At higher temperatures the most probable value $\hat{v}$ is less higher and shifted to the right and the velocity distribution gets wider on the velocity axes, because the area below the graph needs to be normalized.

2.5 Non-dispersive infrared (NDIR) gas sensor

Technique

This technique is used for gas sensing. It is based on infrared spectroscopy, by which the molecules absorb energy at resonant frequencies. Every molecule has different vibrational

frequencies, with this knowledge the molecules can be distinguished from each other. The frequency for which it is resonant depends on the vibrational movement of the molecules. In figure 2.3 the different possibilities of a CO_2 molecule to vibrate are shown. Vibrational movements can be described with the Lorentz model where the atoms act like if they were connected with springs. Every movement has its own resonance frequency which is shown in figure 2.4. The movements are described in figure 2.3: a) the asymmetric stretch where the carbon and oxygen atoms are moving in one plane but in different directions is shown, b) the symmetric stretch where only the oxygen atoms are moving is shown and c) the two degenerated bends where the molecule is moving is shown.

The infrared spectrum in figure 2.4 shows which peaks are assigned to which movement. The central dip belongs to the asymmetric movement which means at this wavenumber the transmittance is very high [28]. The degenerated bends are absorbing infrared light at a much lower wavenumber compared to the asymmetric movement which is described by the right dip in figure 2.4.

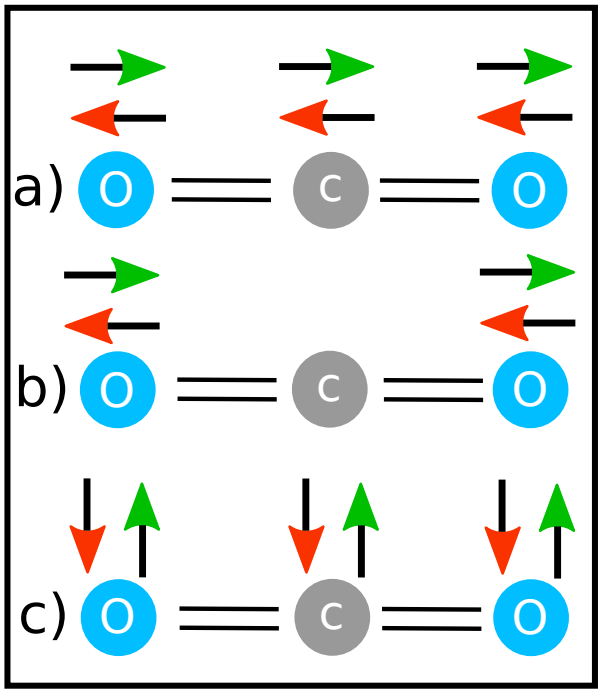

Figure 2.3: The fundamental vibrations of a CO_2 molecule are shown here. From top to bottom: the asymmetric stretch, the symmetric stretch and the degenerated bends.

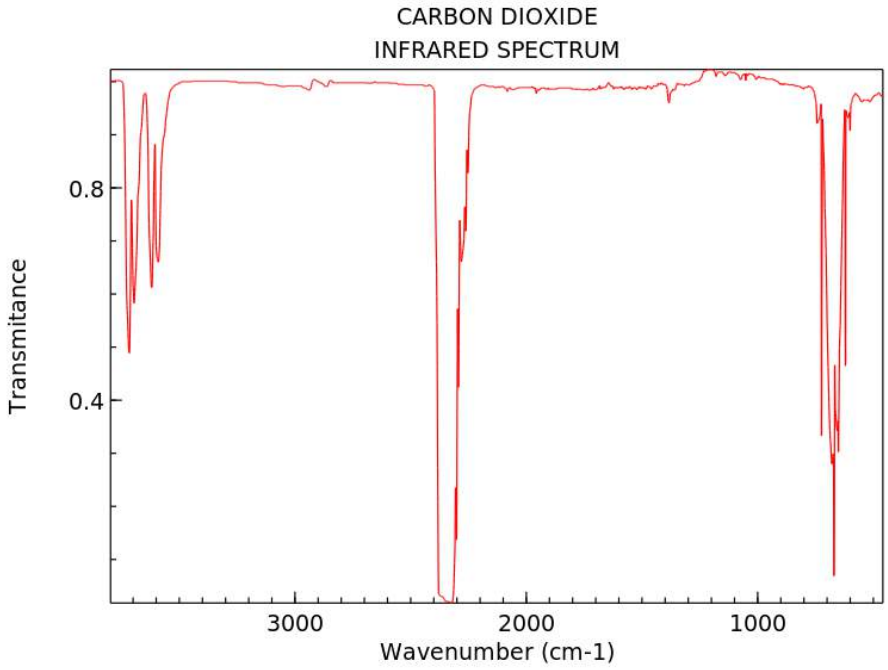

Figure 2.4: Shows the infrared transmission dips for a CO_2 molecule. The two larger dips are approximately at $2325\,\mathrm{cm}^{-1} = 4.3\,\mu\mathrm{m}$ and at $654\,\mathrm{cm}^{-1} = 15.3\,\mu\mathrm{m}$ which are caused by the asymmetric stretch and the degenerated bands [28]. Taken from [26].

Construction

The schematic of the sensor is shown in figure 2.5 as a basic sketch. The gas can enter the chamber at one point and can escape at another point. The infrared source illuminates the chamber up to the other end, where an optical filter and a detector are placed. If the chamber is filled with gas, the infrared source shines through it. The gas absorbs different frequencies, depending on the molecules of the gas. The optical filter is for suppressing the background noises.

The disadvantage of this system is the pressure dependence which influences the absorption measurements. The advantages are that the sensor only has an infrared source and a detector. This advantages results in a small sensor.

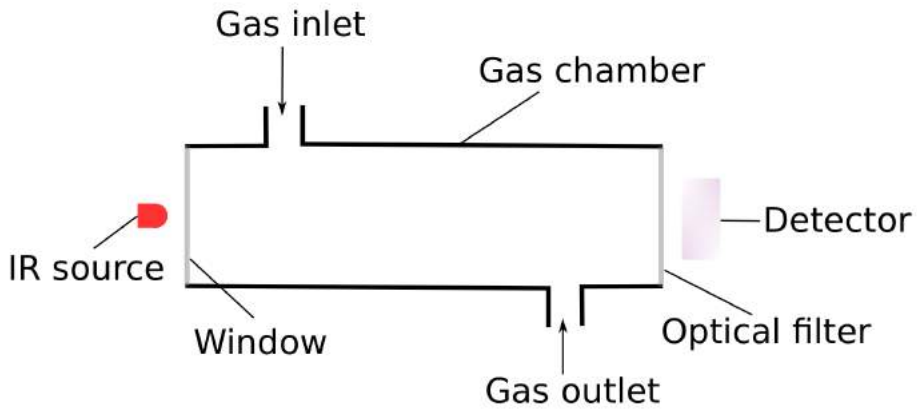

Figure 2.5: Schematic of the CO_2 sensor where the gas enters at one part and escapes at the other one. With an infrared source which illuminates through the chamber it can detect the molecules by absorption. The optical filter helps suppressing the background. After [9].

With the Beer-Lambert law [29], which compares the intensity I_0 from the incoming infrared source and the intensity I from the detector, the equation (2.12) gives the concentration c of the CO_2 gas which depends on the background pressure. I_0 can be determined from the calibration of the sensor.

$$I = I_0 e^{-kcl} \tag{2.12}$$

In equation (2.12) k is the absorption coefficient, and l is the optical absorption path. The concentration can be calculated with equation (2.13).

$$c = \ln\left(\frac{I_0}{I}\right) \cdot \frac{1}{kl} \tag{2.13}$$

2.6 Heat capacity C

The heat capacity C can be derived from the first law of thermodynamics. It represents a material property which depends on the change of the heat Q and temperature T.

First law of thermodynamics

The first law of thermodynamics (2.14) describes the energy change between the internal energy $\mathrm{d}U$, the heat energy $\mathrm{d}Q$ and the work $\mathrm{d}W$.

$$\mathrm{d}U = \mathrm{d}Q - \mathrm{d}W \tag{2.14}$$

The internal energy $\mathrm{d}U$ is composed of the heat energy $\mathrm{d}Q$ and the work $\mathrm{d}W$. Considering a gas in a volume V the internal energy is getting bigger by heating up the gas. The reason is that the particles gain kinetic energy E_{kin}, this energy is divided by three different possibilities to gain energy. These possibilities are defined by the degrees of freedom f which are consisting of a translation, a rotation and a vibration part. As shown in table 2.3, there are differences between monatomic and $N-$atomic molecules. For one atom it is only possible to move in the three-dimensional space, it can't rotate or vibrate. For $N-$atomic molecules, vibrational and rotational degrees of freedom exist. For example, a linear molecule (figure 2.3) like CO_2 has nine degrees of freedom, two rotational and four vibrational degrees of freedom.

Table 2.3: Degrees of freedom f for a atom and a N-atomic molecule

f_i	atom	N-atomic	
		linear	non-linear
translation f_{t}	3	3	3
rotation f_{r}	0	2	3
vibration f_{v}	0	$3N-5$	$3N-6$
total f_{tot}	3	$3N$	$3N$

Derivation

Knowing that changing the heat energy the temperature also changes i.e. $\mathrm{d}Q \sim \mathrm{d}T$, the proportionality factor C is called heat capacity (2.15).

$$C = \frac{\mathrm{d}Q}{\mathrm{d}T} \tag{2.15}$$

The heat capacity is a material property, hence it depends on the mass m. The mass dependency is shown in equation (2.16) which is called specific heat capacity.

$$c = \frac{C}{m} = \frac{1}{m}\frac{\mathrm{d}Q}{\mathrm{d}T} \tag{2.16}$$

A distinction can be made between the specific heat capacity for constant pressure c_p and constant volume c_V.

3 Setup

The setup consists of different parts, four mass flow controllers (MFC), a gas pipe system, valves and a CO_2 sensor, which depend on each other. The main part is the gas pipe system, where the gas first flows through the pipes to the MFCs to be mixed and then from the MFCs to the CO_2 sensor where the gas is then transported away by the gas extraction. The pipes and pipe connections have been selected to be suitable for laminar flow by calculating the Reynolds number and the Knudsen number. One requirement for this setup is a constant mass flow which can be generated with so-called mass flow controllers from MKS. This requirement comes from the fact that the setup is designed for an NO sensor which requires a constant mass flow and should measure low concentrations. Another requirement is that a dilution factor of 10000 should be achievable, the range in which these MFCs should be able to mix is the ppb range, clarified in percentage it is 0.000 000 1 %.

This setup is constructed for the gases NO and N_2 which means that the different parts have to be leak-proof and resistant otherwise NO reacts directly with O_2 to NO_2 which is very toxic. The gas paths were chosen so that NO is not able to get into the N_2 gas container, as these components are not designed for NO where only N_2 should pass. Since the gases NO and N_2 should not be mixed before the MFCs, valves are used to prevent this. Therefore, only the gases N_2 and CO_2 were used for testing. For this setup, a CO_2 sensor is used to investigate the MFCs.

3.1 Mass flow controllers (MFC)

The mass flow is controlled by the MFCs. They are an important part in this setup to produce a continuous controlled mass flow. To get as much variety as possible in mass flow the flows should be adjustable. As an overview, table 3.1 shows the available MFCs with the given flow ranges. These four MFCs were chosen so that the respective flow areas can overlap and thus the system can go from 0.1 sccm to 52 105 sccm.

Figure 3.1 shows a MFC, it has one inlet and one outlet for the gas, and at the top part a D-Sub plug and an Ethernet connection. Two LEDs, also at the top, indicate the status of the MFC.

Figure 3.1: Mass flow controller from MKS, taken from [14]

Table 3.1: Flow ranges of the MFCs

MFCs	Flow ranges
MFC1	1000 to 50000 sccm
MFC2	40 to 2000 sccm
MFC3	2 to 100 sccm
MFC4	0.1 to 5 sccm

A closer look at the inside of a MFC in figure 3.2 shows how it is built. First of all, the flow path of the gas goes through the entry and splits into two parallel ways. One way is through the bypass which is adjustable and the other is through the sensor pipe. After that, both ways are recombined and lead through the control valve to the outlet.

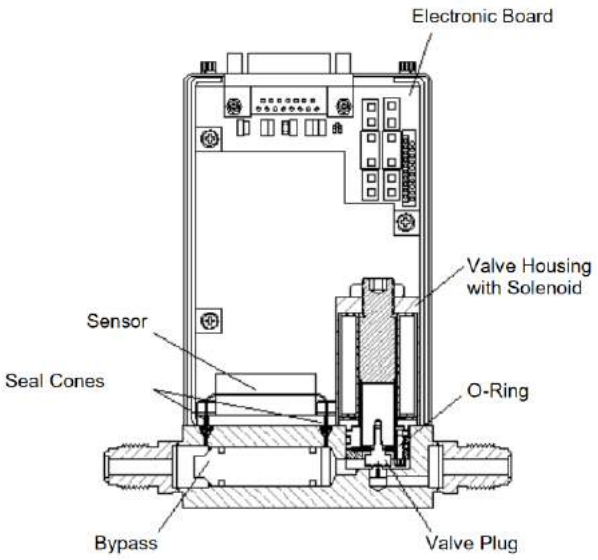

Figure 3.2: Assembly of the MFCs from MKS. It works by measuring the thermal mass movement which than can be concerted with the specific heat capacity c_p to obtain the mass flow. The gas flows from the left to the right side. Taken from [15].

The measurement technique, which is formulated in [15], is based on measuring the thermal mass movement with heat transfer between temperature sensing elements, which than can be converted with the specific heat capacity c_p to obtain the mass flow. By amplifying, digitalising and linearizing the signal it is sent to the control section where it is transform in a $0 - 5\,\mathrm{V}$ analog signal which can be read out.

3.2 Gas pipe system

The basic idea is to build a setup for N_2, NO and N_2/NO 100 ppm or even lower (10 ppm) gas, with four MFCs. Looking at figure 3.3, the basic idea of this setup is shown. Two different gas inlets are used here, because the NO should not be able to get into the N_2 gas container, as these components are not designed for NO, a leak can be dangerous for the experimenters because its react directly with O_2 into the red-brown nitrogen dioxide NO_2. It is to be recognized that the NO gas course only goes to the three lower MFCs because the amount of required total flow is covered with the lower ones.

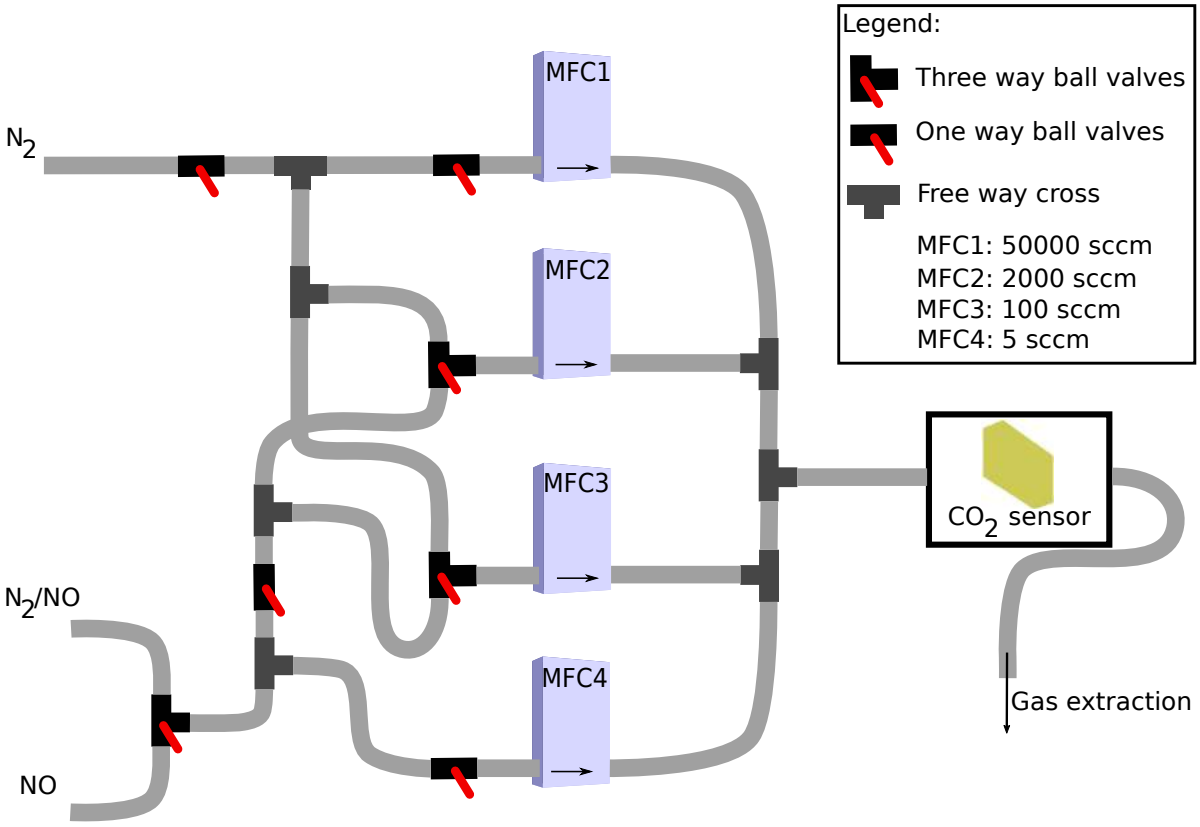

Figure 3.3: It is illustrated the gas pipe setup with MFCs, CO_2 sensor, valves and free way crosses with two inlets. The gases can flow through the MFCs to the CO_2 sensor which measures the concentration and the gas extraction transports the gas out of the system.

Pipes

As calculated in table 2.1 and 2.2, it is possible to choose different diameters for laminar flow in the pipes. In this experiment, an outer diameter of $d = 6$ mm and an inner diameter of $d = 4$ mm is used. An important requirement about these pipes is that they are seamlessly made of stainless steel which makes them more stable for high pressures.

Figure 3.4: Shown are here stainless steel pipes which are seamless [21]

Pipe connections

Cutting rings are very important components in this setup, they seal the screw cap between every pipe to MFC connections and also pipe to valve connections. Two different cutting rings were used here. The first one is from Landefeld, shown in figure 3.5 and the second one is from Swagelok, illustrated in figure 3.6. They are slightly different from each other. The rings from Landefeld are one-piece, while the ones from Swagelok are in two parts. They are sitting in between the pipe and the union nut, by tighten the union nut up, the cutting rings are cutting themselves in the pipe which seals everything.

Figure 3.5: Shown here is a cutting ring from Landefeld [22].

Figure 3.6: Shown here is a cutting ring from Swagelok with union nut[24].

3.3 Valves

Three way ball valve

The three way ball valve in figure 3.7 is an NO resistant valve sealed with PTFE. In the center of the valve a ball is located, which gives the direction of the flow. The ball is not completely filled, the part which is missing gives the opening of the valve. The direction of the flow depends on the borehole, this three way ball valve have a L-drilling which is important because NO shouldn't get a chance to get to the N_2 container.

With the handle at the top, the ball can be moved in the desired direction. A three way ball valve is used in figure 3.3 wherever the different gases can't collide with each other.

Figure 3.7: Shown is here a three way ball valve [16]

One way ball valve

The one way ball valve is similar to the three way ball valve, the difference is that the one way ball valve has only the setting opened or closed. The entrance is regulated with a ball like the three way ball valve.

3.4 CO_2 sensor

The CO_2-sensor (figure 3.8) is a non-dispersive infrared sensor from the brand *Zhengzhou Winsen Electronics Technology Co., Ltd*, Model: MH-Z19B. The pin assignment is shown in figure 3.8 b), a closer look on that shows there are two ways to read the data: quasi analog (**PWM**) and digital (**UART**). The required pins for the **UART**-measurement are Tx and Rx which are transmitter and receiver.

The two white areas in figure 3.8 a) are the inlet and the outlet where the gas can enter and leave the sensor.

The sensor can be zero calibrated by connecting the HD pin with the low level V_0 pin at least for seven seconds.

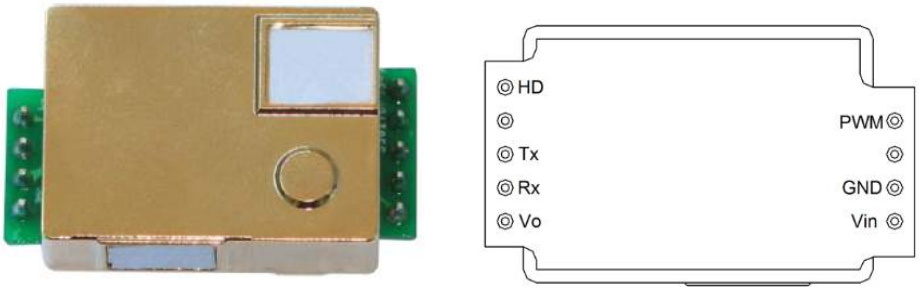

(a) CO_2 sensor (b) Pin assignment

Figure 3.8: A CO_2 sensor from the brand *Zhengzhou Winsen Electronics Technology Co., Ltd* with the model number MH-Z19B[23]

Measuring with *UART*

The measurements by using **UART** were recorded with an Arduino Nano by using the script from [25] which can be found in appendix 1.

The measuring process was as follows: The first thing to do is to calibrate the sensor, which is done by connecting pins HD and V_0 and these for seven seconds when the sensor is connected, which then has to be left for about twenty minutes. After the calibration, the sensor is connected to the Arduino to establish a connection. For the required gas flow, the gas valves are set in the required position and the gas is let through. So that the sensor can measure the concentration, the MFCs are set to the desired setting, now the sensor should be able to measure something. The script from Chapter appendix 1 is executed so that the sensor measures the concentration of CO_2 in [ppm].

4 Measurements and evaluation

The aim of this chapter is to achieve the best combination of MFCs with minimum error. Starting with basic equations in chapter 4.3 and continuing with the error values of the components 4.1, the total flow and the dilution of the MFCs can be calculated. Chapter 4.2 shows the behavior of the MFCs and the CO_2 sensor and finally in chapter 4.3 the choice of the right combination for the MFCs will be discussed.

4.1 Error values of the components

The main error value comes from the CO_2 sensor which is much higher than the one from the MFCs. In the following, the error values of the Sensor and the MFCs will be described.

CO_2 sensor

The accuracy ΔS of the CO_2 sensor is formulated in equation (4.1) and can be found in the data sheet [23].

$$\Delta S = \pm\,(50\text{ppm} + 5\%\text{ of reading value}) \tag{4.1}$$

Section 4.2 shows the accuracy for the values which mostly originate from the sensor.

For the difference D (4.2) between the values of the CO_2 sensor and MFCs, the error can be calculated with equation (4.3). The difference D consists of the CO_2 sensor value and the values from the MFCs, which are given in [sccm], for the two gases which is multiplied with 10^6 due to the unit from the CO_2 sensor, it is in [ppm].

$$D = S_{\text{ensor}} - \frac{\text{CO}_2}{\text{N}_2} 10^6 \tag{4.2}$$

$$\Delta D = \frac{\partial D}{\partial \text{CO}_2}\Delta\text{CO}_2 + \frac{\partial D}{\partial \text{N}_2}\Delta\text{N}_2 + \frac{\partial D}{\partial S}\Delta S \tag{4.3}$$

MFCs

The MFCs have the accuracy [14]

- $\pm$ 1% of set point for 20 to 100% Full Scale and

- ± 0.2% of Full Scale for 2 to 20% Full Scale

With the equation for the MFCs (4.4), which gives the mixing ratio in [ppm], is used for the evaluation, the error can be calculated with equation (4.5).

$$M = \frac{\mathrm{CO_2}}{\mathrm{N_2}} 10^6 \tag{4.4}$$

$$\Delta M = \left(\frac{1}{\mathrm{N_2}} \Delta \mathrm{CO_2} + \frac{\mathrm{CO_2}}{{\mathrm{N_2}}^2} \Delta \mathrm{N_2} \right) 10^6 \tag{4.5}$$

The MFCs have some restrictions as their control range is 2% to 100% of full scale for N_2, for any other gases this value can be slightly different, which depends from the gas type. This difference results from the specific heat capacity c_p which is gas dependent.

4.2 Measurements

In the following the investigation of the CO_2 sensor and the MFCs is given. Questions like "Does the flow change by using different MFCs?" or "Does the CO_2 sensor have some time delay?" will be clarified. The error bars listed here are calculated as described in chapter 4.1.

The measuring process is as follows: First of all, the CO_2 sensor is connected to the Arduino, which evaluates the data. Additionally the CO_2 sensor needs a separate power connection. Then by programming the Arduino with appendix 1, the sensor can be read out. The time and the concentration were read out for the following evaluations. The readout of the MFCs which gives the mass flow for the gases N_2 and CO_2 can be accessed via the website.

Time delay Δt of the CO_2 sensor

When measuring the time delay Δt, the CO_2 concentration and the time t are measured. By changing the CO_2 concentration the CO_2 sensor needs a certain time to get to its final value. For three concentration changes, figure 4.1 shows how much time the sensor needs to reach the final value. The time differences Δt_i in figure 4.1 are $\Delta t_{2\to1} = 407\,\mathrm{s}$, $\Delta t_{4\to3} = 448\,\mathrm{s}$ and $\Delta t_{6\to5} = 481\,\mathrm{s}$. These values are pretty similar to each other which suggests that the time delay is constant. The long time delay comes from the fact that it takes time to have a set equilibrium concentration in the chamber. A disadvantage about this is that the concentration change can't be done fast.

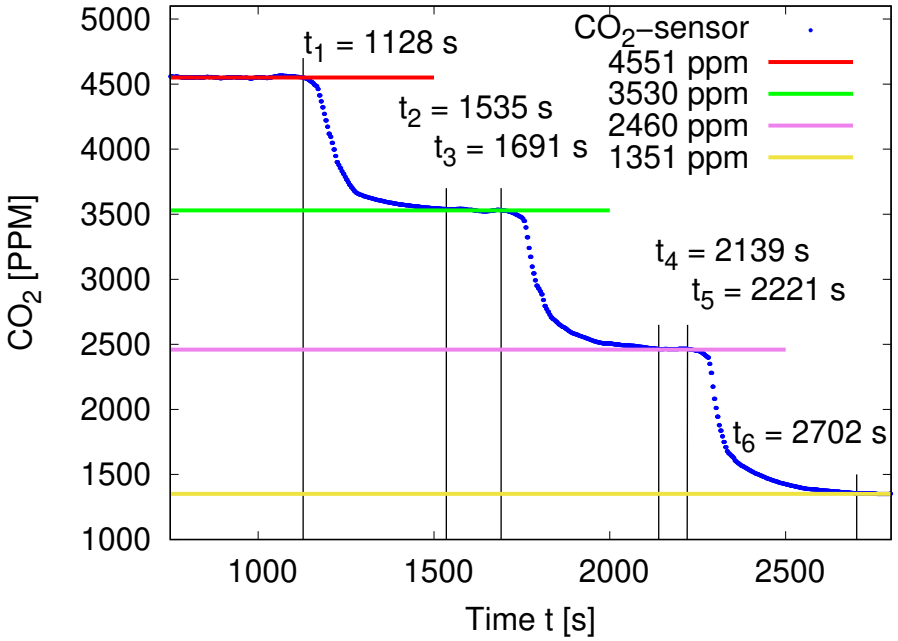

Figure 4.1: Demonstration of the time delay of the CO_2 sensor for different concentration changes plotted against time t. The time delays are: $\Delta t_{2\to1} = 407\,\mathrm{s}$, $\Delta t_{4\to3} = 448\,\mathrm{s}$ and $\Delta t_{6\to5} = 481\,\mathrm{s}$.

Investigation of different MFC combinations for concentrations of 4000 ppm **and** 2000 ppm

For this part, the concentration of the MFCs and the sensor were read out and the difference D was calculated from these values and plotted against the total flow f_{tot}. The difference D describes the difference between the value of the MFCs and the value of the CO_2 sensor this is done because the calibration of the CO_2 sensor is not accurate enough which makes a different between the sensor and the MFCs.

This measurement was done for different combinations of two MFCs, MFC1 = 50 000 sccm and MFC3 = 100 sccm were combined and MFC2 = 2000 sccm and MFC4 = 5 sccm were used together, with concentrations of 4000 ppm and 2000 ppm.

In figure 4.2 it is shown how much the combination of the MFCs affects the difference D for a concentration of 4000 parts per million (ppm) CO_2. The combination of the MFCs is shown in the legend with the associated mass flow rate, N_2 to CO_2. Besides, sccm defines a unit which is called *standard cubic centimeter per minute* ($\mathrm{cm}^3/\mathrm{min}$).

No trend can be observed in the images 4.2 and 4.3 which means that the flow is not changing for different MFC combinations. It should be noted, however, that the error

bars in the figures are very large, which may result in a different looking figure when using a better sensor with lower errors.

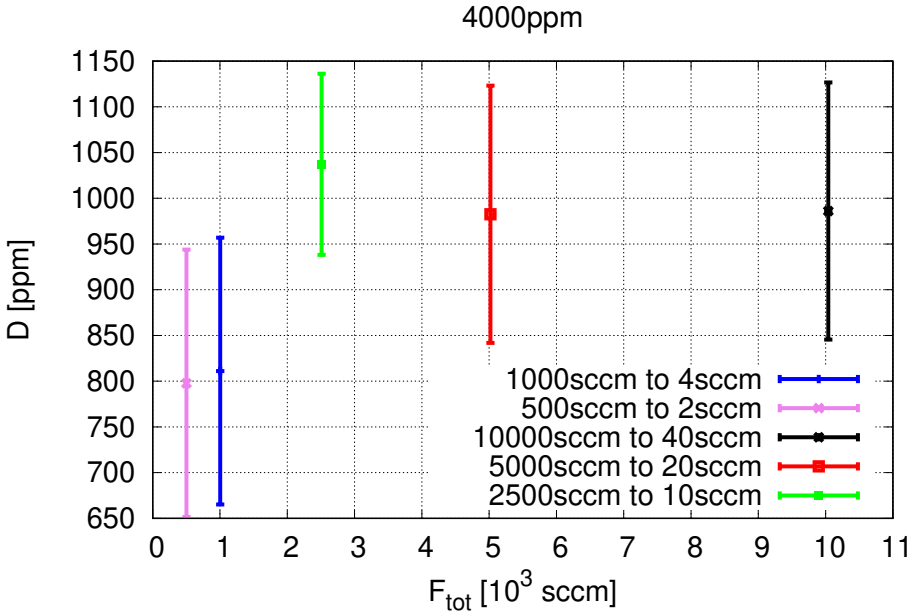

Figure 4.2: Difference D against the total flow f_{tot} for a concentration of 4000 ppm CO_2. The concentration of the MFCs and the sensor were read out and the difference was calculated from these values and was plotted against the total flow. The different combinations of MFCs are shown in the legend of the figure whereby the flow rate is represented as NO to CO_2.

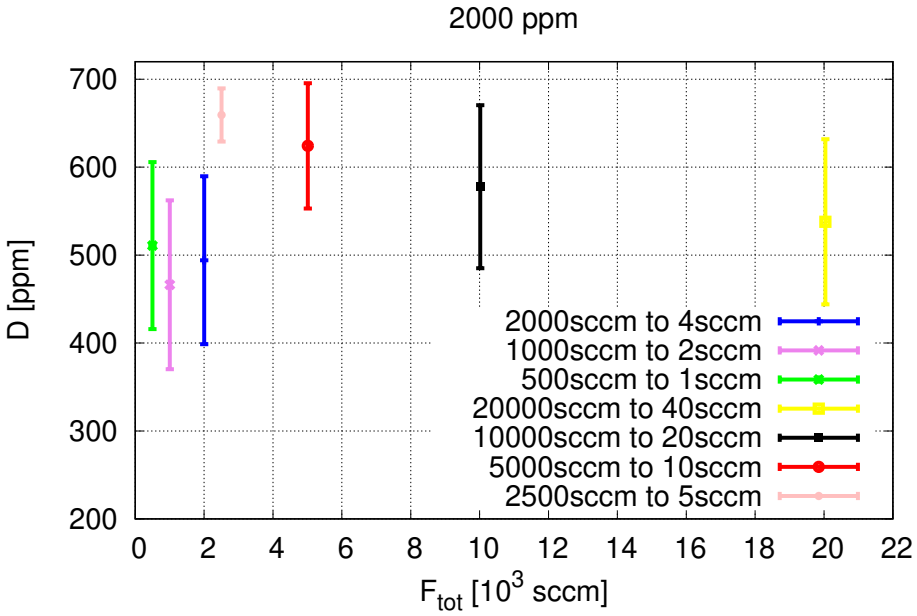

Figure 4.3: Difference D to the total flow f_{tot} for a concentration of 2000 ppm CO_2. The concentration of the MFCs and the sensor were read out and the difference was calculated from these values and was plotted against the total flow. The different combinations of MFCs are shown in the legend of the figure whereby the flow rate is represented as NO to CO_2.

Dependence of the concentration on the ramp direction

At this section, the concentration of the MFCs and the CO_2 sensor were read out and the difference D was calculated from the values and was plotted against the total flow F_{tot}. This was done for concentrations of 4000 ppm, 3000 ppm, 2000 ppm, 1000 ppm and 500 ppm of CO_2 to N_2. For a constant flow of $N_2 =$ 1000 sccm, CO_2 was changed so that the concentration as shown in the figure 4.4 was reached. The time it took until the concentration leveled off can be read off from section 4.2, this time was necessary to wait.

Figure 4.4 shows the results. The chronological order of this measurements is the following: first red dots from 4000 sccm down to 500 sccm and second blue dots back again from 1000 sccm to 4000 sccm. Figure 4.4 shows that comparing both functions there are significant differences in the slope and the axis intercept of the fit function can be recognized, but due to the large error bars it looks as if this was due to the measurement error of the sensor.

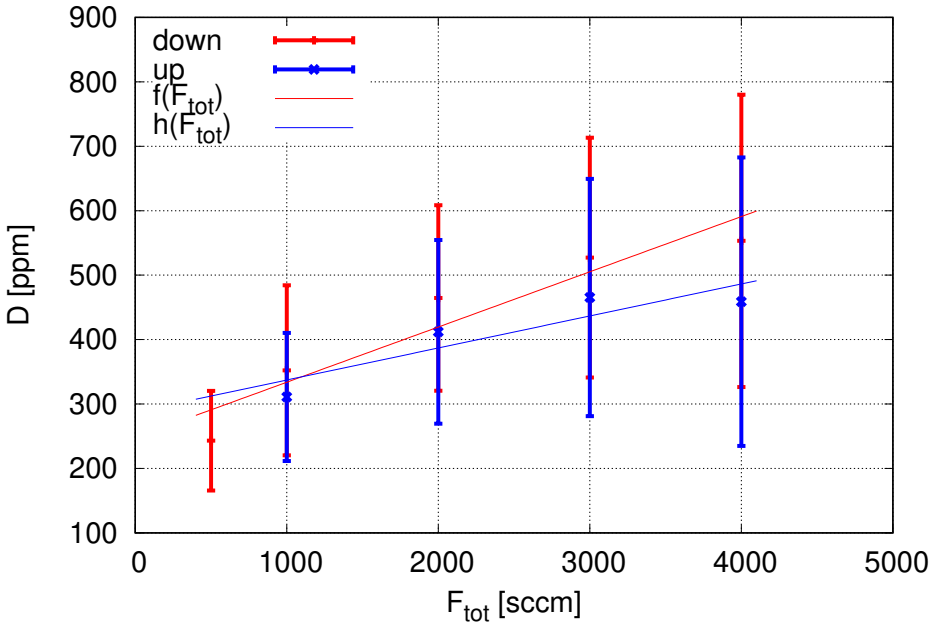

Figure 4.4: Ramping the concentration from low total flow to high total flow (blue) and vice versa (red). The difference between the MFC and the sensor was calculated and shown here. The red dots are going from a flow of 4000 sccm down to 500 sccm and the blue dots back again from 1000 sccm to 4000 sccm, for concentrations of 4000 ppm, 3000 ppm, 2000 ppm, 1000 ppm and 500 ppm. The fit functions are: $f(F_{\text{tot}}) = 0.123\,403\,\text{ppm/sccm} \cdot F_{\text{tot}} + 169.801\,\text{ppm}$ and $h(F_{\text{tot}}) = 0.155\,424\,\text{ppm/sccm} \cdot F_{\text{tot}} + 248.988\,\text{ppm}$.

4.3 Mathematical treatment of the dilution and total flow

At this point in the evaluation, a mathematical consideration is made which estimates an error and minimizes it. The CO_2 sensor is not taken into account, because the minimization of errors of the MFCs are simulated.

In this there are few important equations like the total flow F_{tot} (4.6) and the dilutions D_i (4.7), (4.8), (4.9). The dilution describes a ratio, e.g. D_2 has considered a ratio between flow of NO to total flow F_{tot}. x_i can assume values from 0.02 to 1.

The total flow F_{tot} is defined as the sum over all MFCs with the maximum flow range (table 3.1) multiplied with x_i which gives the percentage of the MFCs divided by 100.

$$F_{\text{tot}} = 50000 \cdot x_1 + 2000 \cdot x_2 + 100 \cdot x_3 + 5 \cdot x_4 \tag{4.6}$$

$$D_1 = \frac{2000 \cdot x_2 + 100 \cdot x_3 + 5 \cdot x_4}{F_{\text{tot}}} \tag{4.7}$$

$$D_2 = \frac{100 \cdot x_3 + 5 \cdot x_4}{F_{\text{tot}}} \tag{4.8}$$

$$D_3 = \frac{5 \cdot x_4}{F_{\text{tot}}} \tag{4.9}$$

MFC setting with minimal error

When looking at the MFCs, they have the following error, which depends on the set flow [14]

- ± 1% of set point for 20 to 100% Full Scale
- ± 0.2% of Full Scale for 2 to 20% Full Scale

To obtain a minimum error for different combinations of MFCs, this can be calculated analytically. With using the equations for total flow (4.6), the dilutions (4.7), (4.8) and (4.9) and the error functions which can be generated from the data given from the upper part, a linear system of equations can be formed. The linear system of equations does not provide an unambiguous solution because it is under-determined with two independent equations, with two parameters F_{tot} ans D and three unknowns x_i. The result is a bevy of solutions, which can be infinitely many or none exist.

By using Wolfram Mathematica the script in appendix 2 was solved. The figures 4.5, 4.6 and 4.7 were created with this script. The figures show different combinations of MFCs with a total flow of $F_{\text{tot}} = 1000\,\text{sccm}$ and a dilution of $D_2 = 1/1000$. The dark violet spots indicate a small error ranging up to yellow spots as the larger error range.

Figure 4.5 shows perfectly that smaller errors are obtained by choosing larger MFC in the upper range, than the smaller ones in this range, which is also illustrated in figures 4.6 and 4.7. For the setup it means to rather choose a combination where the bigger one is more open compare to the other one to have a larger full scale which minimize the total error.

These pictures only shows one way to combine the MFCs for a total flow of $f_{\text{tot}} = 1000\,\text{sccm}$. This script can go through any number of options by changing the total flow f_{tot} and the dilutions D_i.

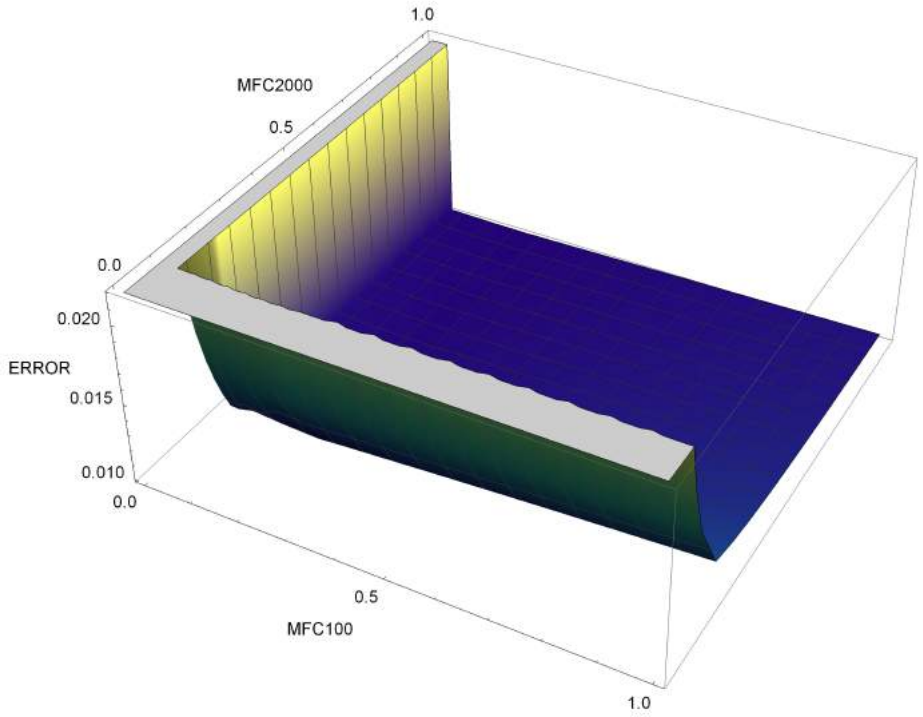

Figure 4.5: The combination here is with the MFC2 = 2000 sccm and the MFC3 = 100 sccm, for this the script in Chapter 2 was carried out by Mathematica for a total flow of $f_{\text{tot}} = 1000$ sccm and the dilution of $D_2 = 1/1000$ assumed. The two MFCs are shown in the percentage range of 0% to 100% for 0% as closed and 100% as completely opened and the associated error $ERROR$ in sccm, which is shown as a height map.

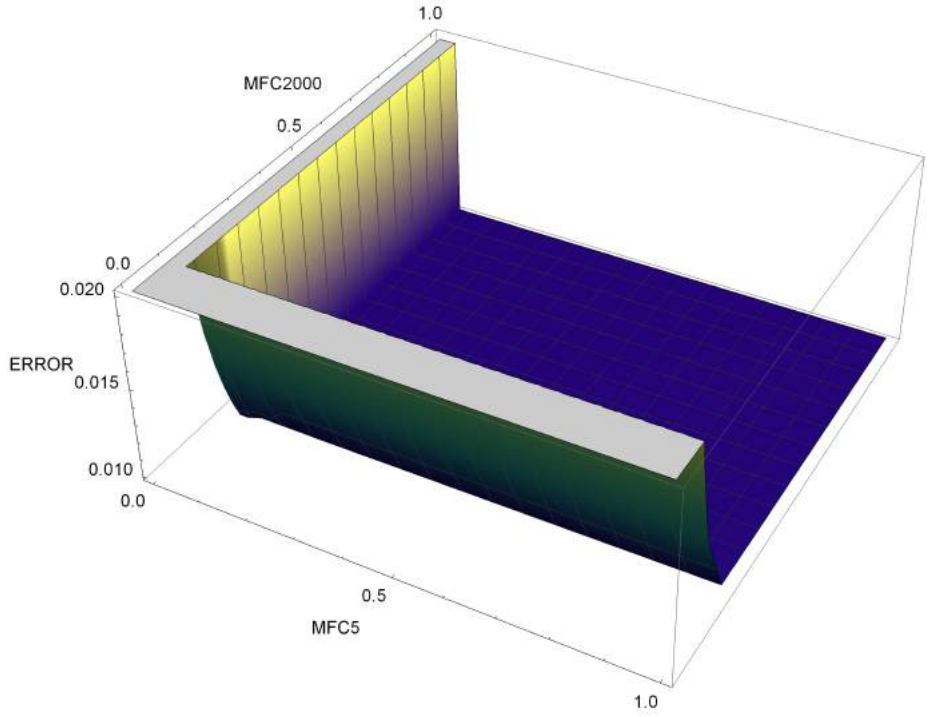

Figure 4.6: The combination here is with the MFC2 = 2000 sccm and the MFC4 = 5 sccm, for this the script in Chapter 2 was carried out by Mathematica for a total flow of $f_{\text{tot}} = 1000$ sccm and the dilution of $D_2 = 1/1000$ assumed. The two MFCs are shown in the percentage range of 0% to 100& for 0% as closed and 100% as completely opened and the associated error $ERROR$ in sccm, which is shown as a height map.

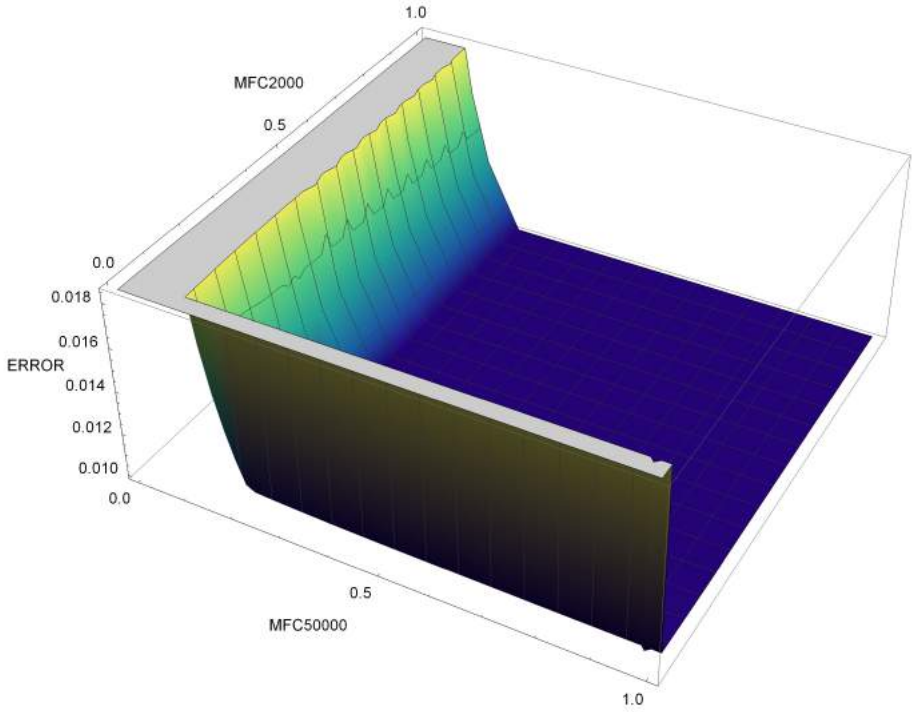

Figure 4.7: The combination here is with the MFC2 = 2000 sccm and the MFC1 = 50 000 sccm, for this the script in Chapter 2 was carried out by Mathematica for a total flow of $f_{\text{tot}} = 1000$ sccm and the dilution of $D_2 = 1/1000$ assumed. The two MFCs are shown in the percentage range of 0% to 100% for 0% as closed and 100% as completely opened and the associated error $ERROR$ in sccm, which is shown as a height map.

5 Conclusion and outlook

The aim of this work was to set up and plan a gas mixing system for the gases NO and N_2. The system was checked with CO_2 gas which is less toxic and less expensive to NO, and which was measured with a CO_2 sensor. Since the structure is assembled with pipes, the diameter d should be determined for these, which is done in chapter 2 with the calculation of the Knudsen number Kn and the Reynolds number Re.

For a laminar flow, a diameter of $d = 4\,\text{mm}$ can be assigned in this setup. For a constant flow, mass flow controllers (MFCs) are used to create different mixing ratios. The mode of operation is considered in section 3.1, it is based on measuring the thermal mass movement which than can be concerted with the specific heat capacity c_p to obtain the mass flow. To measure the concentration after the MFCs, a CO_2 sensor is used, which measures infrared absorption of the molecules and it is explained in more detail in chapter 3.4. For the investigation of the system, which is designed for N_2 and NO gas, measurements are made with CO_2 and N_2 gas because it is easier to handle than NO gas.

In chapter 4 *Measurements and evaluations*, the MFCs and the CO_2 sensor are examined. During the examination of the CO_2 sensor while recording the data, it was noticed that the long time delay Δt comes from the fact that it takes time to have a set equilibrium concentration in the chamber which is not optimal since the recordings cannot be changed after any time. The MFCs were taken into account when examining the combinations for constant concentrations, which has resulted in the fact to be observed for 2000 ppm and 4000 ppm of CO_2 in relation to the total flow F_{tot}. In all measured data, the CO_2 sensor has a very high influence on the error bars, which consist almost entirely of the sensors error, which does not simplify the evaluation of the MFCs.

The script in appendix 2, which was solved with Mathematica, offers a solution for the MFCs, here, the combinations of MFCs are considered without the sensor, the images in section 4.3 are shown for this. The figures clearly show the smallest error for every two combined MFCs for a total flow of $f_{\text{tot}} = 1000\,\text{sccm}$ and a dilution of $D_2 = 1/1000$.

The next task to work on is to use this gas mixing system for the optogalvanic sensor, the CO_2 sensor is removed.

At the moment there are problems to bring the parameters under control, like the pressure fluctuations in the measuring system, which makes the investigations unreliable. The first step is to tested it with pure N_2 to look if the pressure is stable. If the measurements are accordingly to what the expectation is the setup is used for NO and the mixing ratios are set.

1 CO_2 sensor

In the following, the script from [25] was presented in a brief version.

```
#include <SoftwareSerial.h>

// Port 2 (RX) and Port 3 (TX)

SoftwareSerial co2Serial(2, 3); // define MH-Z19 RX TX

void setup() {

  Serial.begin(9600);
  co2Serial.begin(9600);

}

// Reading out the sensor values ppm and temperature

void loop() {

  int ppm, temperature = 0;
  readSensor(&ppm, &temperature);

//  Serial.print("PPM: ");
  Serial.print(ppm);
  Serial.print("  ");
  Serial.println(temperature);

  delay(1000);
}

void readSensor(int *ppm, int *temperature){

  byte cmd[9] = {0xFF,0x01,0x86,0x00,0x00,0x00,0x00,0x00,0x79};
  byte response[9];
  co2Serial.write(cmd, 9);
  memset(response, 0, 9);
  while (co2Serial.available() == 0) {
    delay(100);
  }

  co2Serial.readBytes(response, 9);
  byte check = getCheckSum(response);

  if (response[8] != check) {
    Serial.println("Fehler in der   bertragung  !");
    return;
  }

  *ppm = 256 * (int)response[2] + response[3];
  *temperature = response[4] - 40;

}
```

```
byte getCheckSum(byte *packet) {
  byte i;
  byte checksum = 0;
  for (i = 1; i < 8; i++) {
    checksum += packet[i];
  }
  checksum = 0xff - checksum;
  checksum += 1;
  return checksum;
}
```

2 Choice of MFCs

```
Remove["Global`*"]


Flow[max_, x_] := max*x;
Error[max_, x_] := If[x == 0,0,If[x > 1,10^10,
                   If[x < 2/100,10^10,
                   If[x < 2/10,2/1000*max,x*1/100*max]]]];

GesFlow = Flow[50000, f50000] + Flow[2000, f2000]
        + Flow[100, f100] + Flow[5, f5];

ErrorFlow = Error[50000, f50000] + Error[2000, f2000]
          + Error[100, f100] + Error[5, f5];

D1 = (Flow[2000, f2000] + Flow[100, f100] + Flow[5, f5])/GesFlow;
D2 = (Flow[100, f100] + Flow[5, f5])/GesFlow;
D3 = (Flow[5, f5])/GesFlow;

ErrorD1 = (2*ErrorFlow - Error[50000, f50000])/GesFlow;
ErrorD2 = (2*ErrorFlow - Error[50000, f50000] - Error[2000, f2000])/GesFlow;

Restriction = f50000 < 1 && (f50000 >= 0.02 || f50000 == 0) &&
              f2000 < 1 && (f2000 >= 0.02 || f2000 == 0) &&
              f100 < 1 && (f100 >= 0.02 || f100 == 0) &&
              f5 < 1 && (f5 >= 0.02 || f5 == 0);



sols = Solve[{GesFlow == 1000, D2 == 1/1000, Restriction},
             {f50000, f2000, f100, f5}]



sols[[1]]

Plot3D[ErrorD2 /. sols[[1]], {f100, 0, 1}, {f2000, 0, 1} ,
PlotLegends -> Automatic, AxesLabel -> {MFC100, MFC2000, ERROR},
ColorFunction -> "BlueGreenYellow",
LabelStyle -> Directive[FontFamily -> "Arial", FontSize -> 15]]

Plot3D[ErrorD2 /. sols[[1]], {f5, 0, 1}, {f2000, 0, 1},
PlotLegends -> Automatic, AxesLabel -> {MFC5, MFC2000, ERROR},
ColorFunction -> "BlueGreenYellow",
LabelStyle -> Directive[FontFamily -> "Arial", FontSize -> 15]]

Plot3D[ErrorD2 /. sols[[1]], {f50000, 0, 1}, {f2000, 0, 1},
PlotLegends -> Automatic, AxesLabel -> {MFC50000, MFC2000, ERROR},
ColorFunction -> "BlueGreenYellow",
LabelStyle -> Directive[FontFamily -> "Arial", FontSize -> 15]]
```

Bibliography

[1] SCHMIDT, Johannes, et al. Proof of concept for an optogalvanic gas sensor for NO based on Rydberg excitations. Applied Physics Letters, 2018, 113. Jg., Nr. 1, S. 011113

[2] Moncada S. Nitric oxide: discovery and impact on clinical medicine. J R Soc Med. 1999 Apr;92(4):164-9. doi: 10.1177/014107689909200402. PMID: 10450191; PMCID: PMC1297136.

[3] GROB, Natalia M.; DWEIK, Raed A. Exhaled nitric oxide in asthma: progress since the introduction of standardized methodology. Journal of breath research, 2008, 2. Jg., Nr. 3, S. 037002.

[4] Karl Jousten Hrsg. Handbuch Vakuumtechnik 12. Auflage

[5] https://www.uni-due.de/pc-sa/lehre/Vorlesung_NWGIWI_161-170-s-w.pdf (29.09.2020)

[6] The Vacuum Technology Book, Volume II, Pfeiffer Vacuum

[7] https://chem.libretexts.org/Bookshelves/Physical_and_Theoretical_Chemistry_Textbook_Maps/Supplemental_Modules_(Physical_and_Theoretical_Chemistry)/Kinetics/03%3A_Rate_Laws/3.01%3A_Gas_Phase_Kinetics/3.1.02%3A_Maxwell-Boltzmann_Distributions (30.09.2020)

[8] HUSSAIN, Humaira; KIM, JinHo; YI, SeungHwan. Characteristics and Temperature Compensation of Non-Dispersive Infrared (NDIR) Alcohol Gas Sensors According to Incident Light Intensity. Sensors, 2018, 18. Jg., Nr. 9, S. 2911

[9] https://www.dwyer-inst.com/articles/?Action=View&ArticleID=83 (09.10.2020)

[10] https://de.wikipedia.org/wiki/Gassensor#Infrarotoptische_Gassensoren_(NDIR) (09.10.2020)

[11] DINH, Trieu-Vuong, et al. A review on non-dispersive infrared gas sensors: Im-

provement of sensor detection limit and interference correction. Sensors and Actuators B: Chemical, 2016, 231. Jg., S. 529-538

[12] https://wiki.anton-paar.com/kr-kr/infrared-spectroscopy/ (01.11.2020)

[13] https://www.uni-ulm.de/fileadmin/website_uni_ulm/nawi.inst.251/Didactics /thermodynamik/INHALT/REAL.HTM (12.10.2020)

[14] Datasheet for the MFCs from MKS for the model GM50 retrieved from: https://www.mksinst.com/mam/celum/celum_assets/resources/GM50-ds.pdf (13.10.2020)

[15] Introduction manual for digital mass Flow Controller Type 1179B / 1479B / 2179B and digital mass flow meter 179B retrieved from: https://www.mksinst.com/mam/celum/celum_assets/resources/1179Bman.pdf (13.10.2020)

[16] Three way ball valve retrieved from: https://www.edelstahl24.com/armaturen /kugelhaehne-ohne-antrieb/3-wege-mit-iso-top-l-bohrung/3-wege-kugelhahn-mit-iso-anbauplatte-l-bohrung.html (15.10.2020)

[17] http://www.lecksuchtechnik.de/science/einfuehrung-in-die-gasgesetze.html (21.10.2020)

[18] http://www.peacesoftware.de/einigewerte/co2_e.html (21.10.2020)

[19] https://www.tf.uni-kiel.de/matwis/amat/mw1_ge/kap_5/backbone/r5_2_1.html (22.10.2020)

[20] http://www.physik.uni-regensburg.de/forschung/gebhardt/gebhardt_files/skripten /Molekuelabsorption.Heimbach.pdf (22.10.2020)

[21] Datasheet from the stainless steel pipes from landefeld retrieved from: https://www.landefeld.de/cgi/main.cgi?DISPLAY=artikel_datenblattparam_0 =6392 (22.10.2020)

[22] Datasheet from the cutting rings from landefeld retrieved from: https://www.landefeld.de/cgi/main.cgi?DISPLAY=artikel_datenblattparam_0 =2420 (22.10.2020)

[23] Infrared CO_2 sensor datasheet Model: MH-Z19B retrieved from: https://www.reichelt.de/index.html?ACTION=7LA=3OPEN=0INDEX =0FILENAME=X200%2FMH-Z19B_DB_EN.pdf (22.10.2020)

[24] Datasheet from the cutting rings from swagelok retrived from: https://www.swagelok.de/tools%20pages/download_pdf.aspx?part=SS-100-NFSETconfigured=False (27.10.2020)

[25] https://www.blikk.it/forum/blog.php?bn=neuemedien_fblang=deid=1575901160 (01.10.2020)

[26] https://webbook.nist.gov/cgi/cbook.cgi?ID=C124389Type=IR-SPECIndex=1 (01.11.2020)

[27] https://pawn.physik.uni-wuerzburg.de/video/thermodynamik/k/sk06.html (02.11.2020)

[28] http://butane.chem.uiuc.edu/pshapley/Environmental/L13/2.html (03.11.2020)

[29] SASSAROLI, Angelo; FANTINI, Sergio. Comment on the modified Beer–Lambert law for scattering media. Physics in Medicine Biology, 2004, 49. Jg., Nr. 14, S. N255

[30] STEBBINGS, R. F., et al. (Hg.). Rydberg states of atoms and molecules. Cambridge University Press, 1983.